# Microstructural Design of the Cast Iron via Laser Hardening with Defocused Beam of the Continuous Wave CO2 Laser



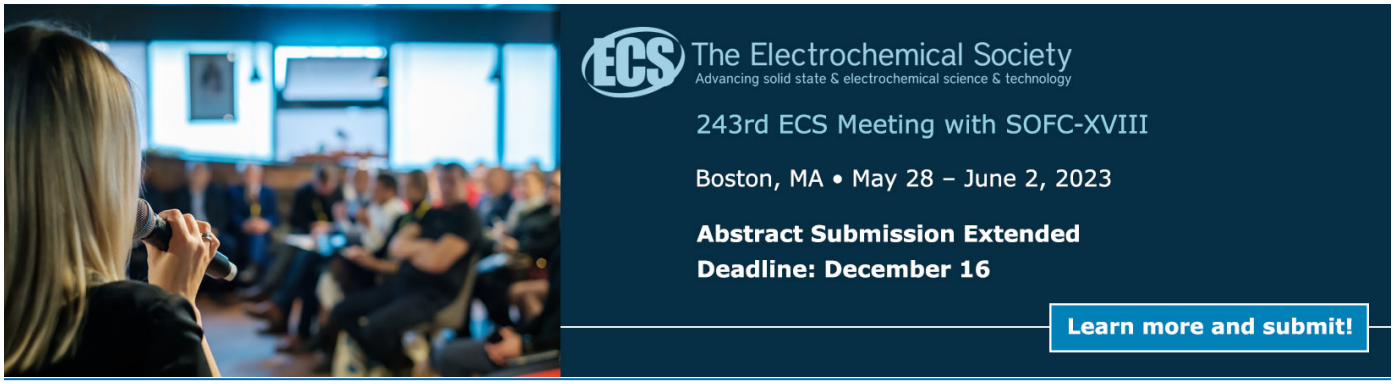

# Microstructural Design of the Cast Iron via Laser Hardening with Defocused Beam of the Continuous Wave CO2 Laser

**J.I. Ahuir-Torres[1], M. Sharp[1], N.Bakradze[2] and A.D.L Batako[1]**

[1] General Engineering Research Institute, Liverpool John Moores University, Byrom street, Liverpool, L3 3AF, UK
[2]Faculty of Transportation and Mechanical Engineering, Georgian Technical University, Georgian, Tbilisi

**Abstract.** The cast iron is widely used in mechanical parts due to its good properties, as damping, good fluidity, resistance to deformation, excellent machinability and low cost. However, the number of its applications are reduced because its low corrosion, wear and friction resistance. The microstructure of the metallic materials has high influence on these properties. Laser hardening can improve these properties via designing of the microstructure. The evaluation of the laser parameter influence on the microstructural features is vital for a correct design of the microstructure and therefore, good improvement of the metallic material properties. Although the various laser parameter influence has been analysed on sundry papers, the influence of the distance from focal point and scan speed in the laser hardening microstructures has been rarely evaluated in the literature. Thus, the influence of this parameter on the microstructures generated through laser hardening is the subject matter of this work. The experiments were carried out with continuous wave carbon dioxide laser on samples of ground cast iron. The atmosphere was air flow at 0.7MPa, the laser operated at 100W and the scan rates were 1mm/s and 5mm/s. The distances to focal point of the laser beams ranged from 0.0mm to 5.6mm. The microstructures of the samples were revealed via nital and evaluated with optical microscopy. This work shown that the microstructure of gray iron cast can be designed by mean of laser hardening. In addition, laser hardened zones had various microstructures (e.g. austenitic, martensitic, pearlite and dendritic). The type of the microstructures in laser treated zones was determined by distance from focal point and scan speed. Moreover, the width and the depth of the laser hardened zones were generally enlarged with the increasing of the distance from focal point. Furthermore, the laser irradiation at slow rates, i.e. 1mm/s, produced laser hardened zones larger than laser scan at 5mm/s. In future works, the hardness, wear and friction resistance of the laser hardened samples will be evaluated because the literature review indicates that austenitic and martensitic microstructures show high values of these properties.

**Keywords:** Cast iron, laser hardening, microstructural change, continuous wave, defocused beam.

## 1 Introduction

Gray cast iron are widely used in various mechanical applications as such disk brake rotors, gear bearings, engine casings and hydraulic valve [1-3]. This is due to its excellent properties as, flexibility in usage, good deformation resistance, excellent fluidity, well castability, low cost and machinability [1, 3-5]. However, the use time of this cast iron in harsh environments is reduced because of its deficiencies as, poor corrosion resistance, low hardness, modest friction and wear resistances [6, 7]. These properties are determined by the microstructure of the metallic materials. Homogeneous and austenitic microstructures had higher corrosion resistance than heterogeneous surfaces [8, 9]. Austenitic and martensitic microstructures present high hardness while pearlite and ferrite microstructure are weaker [4, 6, 7, 10]. Wear resistance is high in mixed structure consisted of austenitic

matrix with martensitic particles [10]. Thus, the modification or design of the microstructure can improve the hardness, corrosion, wear and friction resistance of the grey cast iron.

Laser hardening is powerful technique to improve the physicochemical properties of the materials as such hardness, corrosion, wear and friction resistance, because its excellent qualities as, rapid processing, localized treatment, automatisable and high reproducibility [2, 6, 11, 12]. In addition, the conventional methods, e.g. flame or induction hardening process, need large amount of heat for prolonged period time to obtain the desired microstructure, which is unnecessary in the case of laser hardening [13, 14]. Moreover, other hardening methods have low control in microstructures characteristics, while the control of the laser hardening on microstructure is high [9, 13, 15]. These improvements on the material properties are generated via the microstructural changes with laser radiation. The energy of the laser beam is absorbed by free electrons of the surfaces that are excited to conduction band in the case of metallic materials. Then, electrons are de-energised by mean of their collisions with the atoms of the material. These collision produce the increasing of the temperature of the metallic alloy that can be heat, molted and evaporate the material. After laser impact, metallic material is rapidly cooled by the diffusion of the temperature within material [13, 16]. This laser processing can modify the microstructure of the metallic alloys via these thermodynamic proceedings. The characteristics of the microstructures created via laser hardening, size and type, are strongly influenced by temperature that is reached the material, T, and cooling time, t. These factors are in turn determined by physical chemical properties of the metallic alloy and laser parameters [17]. Thus, the properties of the materials can be improving through the design of the microstructure via adequate combination of the laser parameters. Distance to focal point, Z, and scans speed, v, are important laser parameters on microstructural modifications of the materials.

For these reasons, the present work is a study about the design of the microstructure of grey cast iron through a continuous wave (CW) carbon dioxide ($CO_2$) laser. For this propose, the influence of Z and v on the microstructural features of the laser treated cast iron were evaluated in this work.

## 2 Experimental Setup

### 2.1 *Material*

As-received samples were grey cast iron of type E with a hypoeutetic interdendritic microstructure with graphite flake, can be observed in optical picture of Figure 1. A matrix of α-Fe with cementite ($Fe_3C$) and flake graphite formed the microstructure of this cast iron. Cementite particles were grey spheres while graphite were black flakes. This type of microstructure is often called as pearlite [18].

The samples had 50mm of diameter and 3mm of thickness. Besides, the surfaces of the samples were grinding to avoid the imperfection influence on the laser processing.

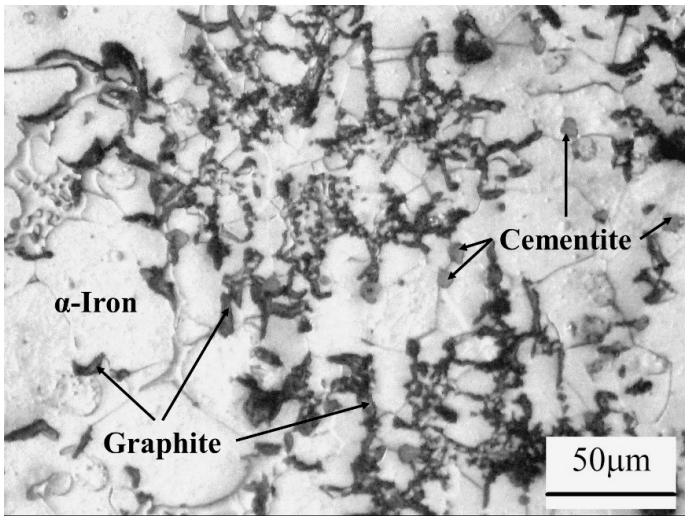


**Figure 1.** Metallographic picture of the grey cast iron type E**.**

Chemical composition of the as-received samples was listed in Table 1 [19].

**Table 1.** Grey cast iron chemical composition

| Element | Fe | C | Si | Mn | Cr | Cr | Ni | Mo | S | P |
|---|---|---|---|---|---|---|---|---|---|---|
| Concentration (%) | Balance | 3.25-3.50 | 1.8-3.0 | 0.50-0.90 | 0.05-0.45 | 0.15-0.40 | 0.05-0.20 | 0.05-0.10 | 0.15 | 0.12 |

The physicochemical properties of the as-received samples are detailed in Table 2.

**Table 2.** Chemical-physic properties of the grey cast iron.

| **Property** | **Value** |
|---|---|
| Density (g/cm$^3$) [19] | 7.200 |
| Specific heat capacity (J/g*K) [19] | 0.490 |
| Thermal conductivity (J/s*cm*K) [19] | 0.533 |
| Thermal diffusivity (cm$^2$/s)$^o$ | 0.127 |
| Molten temperature (K) [19] | 1438.500 |
| Molten enthalpy (J/g) [20] | 240.000 |

$^o$This value was calculated

Thermal diffusivity, β, was calculated via equation 1 [21].

$$\beta = \frac{\delta}{C_p * \rho} \quad (1)$$

Where, δ is thermal conductivity, $C_p$ is specific heat capacity and ρ is density.

## 2.2 *Laser Parameters*

Laser device used in this study was a CW laser of $CO_2$, model *FB1500 flatbed laser cutting system*, which was supplied by *CadCamTechnology Ldt*. The details of the laser system are collected in Table 3.

**Table 3.** Details of the CW $C_2O$ laser.

| **Parameter** | **Value** |
|---|---|
| Wavelength (nm) | 10600.0 |
| Power (J/s) | From 0.0 to 100.0 |
| Scan speed (mm/s) | From 0.2 to 1000.0 |
| Raw beam size (mm) | 4.0 |
| Beam quality | 1.3 |
| Focal length (mm) | 50.0 |
| Focused beam size (μm)* | 219.0 |
| Rayleigh length (mm)* | 2.7 |

Focused beam size, $d_o$, was determined via equation 2 [22, 23].

$$d_o = \frac{4 * M^2 * FL * \lambda}{\pi * D} \quad (2)$$

Being, $M^2$ beam quality, FL focal length, λ wavelength and D raw beam size. Equation 3 [23, 24] was used to calculate the Rayleigh length, $Z_R$.

$$Z_R = \frac{\pi * d_o^2}{\lambda * 4 * M^2} \quad (3)$$

Laser processes were carried out at 0.7MPa air flow through single linear scans with 1mm/s and 5mm/s. Laser device was operating at 100W. Z were from 0.0 to 5.6mm, which were increased 0.8mm. $D_o$, according to Z were estimated by mean of equation 4 and these values are listed in Table 4 [14, 22, 24].

$$D_o = d_o * \sqrt{1 + \left(\frac{Z}{Z_R}\right)^2} \quad (4)$$

**Table 4.** $D_o$ according to Z.

| **Z (mm)** | **Do(μm)** |
|---|---|
| 0 (Focal point) | 219.0 |
| 0.8 | 228.0 |
| 1.6 | 255.0 |
| 2.4 | 293.0 |
| 3.2 | 340.0 |
| 4.0 | 391.0 |
| 4.8 | 447.0 |
| 5.6 | 504.0 |

### 2.3 *Analysis Method*

The microstructures of the samples were developed via the next process of metallography. Firstly, the samples were cut for cross-section. Then, cross-section were grinded via subsequent silicon carbide papers of P320, P600 and P1200. Hereafter, grinded surfaces were polished with consecutive diamond pastes (6μm, 3μm and 1μm) and ending with a polishing of colloidal silica gel dissolution (colloidal silica gel 50% in volume and distilled water 50% in volume). At few minutes after polishing with colloidal silica gel dissolution, cross-sections were etched via 30s of immersion in nital dissolution (2% in volume of nitric acid and 98% in volume of ethanol) [25]. Cleaning processes were conducted after each step of grinding and polishing and, before and after etching. This process was consisted of five stages. First stage, samples were cleaned with commercial detergent and tape water. Following stage, samples were emerged in distilled water. Third stage, the samples were sprayed with isopropanol. In the last stage, samples were fast dried with dryer. Grinding and polishing stuffs were supplied by *Struer*.

The microstructures of the samples were evaluated via optical light microscope, model *BH2-UMA Optical Microcope*, which was supplier by *Olympus Digital Microscope*. The pictures were obtained at 10X, 20X and 50X magnification with *DinoCapture 2.0* software.

## 3 **Results and Discussion**

Laser processing punctually modified the grey cast iron in determined zones, as can be seen in Figure 2. Laser scans at 1mm/s (Fig.2.b, Fig.2d, Fig.2.f, Fig.2.h, Fig.2.i, Fig.2.j and Fig.2.k-n) ablated the metallic alloy while laser scans (Fig.2.a, Fig.2.c, Fig.2.e, Fig.2.g and Fig.2.k) only change the microstructure of the alloy. This indicates that laser scans at 1mm/s evaporated and melted the material whilst laser scans at 5mm/s only produced the molten of the grey cast iron. This is due to laser scans at low speed provide more energy to samples than laser scans at high velocity. Lineal density energy, $E_l$, or energy received by material per area is inversely proportional to scan speed, v, as being viewing in equation 5 [26, 27].

$$E_l = \frac{P}{D_o * v} \quad (5)$$

Where, P is power. As showing this equation, $E_l$ of the laser scans at 5mm/s are lower 5 times than that for 1mm/s laser scans. Obviously, vaporization energy of the cast iron is higher than molten energy. Laser scans at low speed therefore have higher or similar $E_l$ than vaporization energy while high speed laser scans $E_l$ are in the order of the molten energy.

Laser scan at 5mm/s can modify the cast iron until 4.0mm Z while maximum Z was 5.6mm for 1mm/s laser scans. This is due to low v of these laser scans can offset wider $D_o$ than that for high v. The laser scan viability to modify the cast iron microstructure are established by $E_l$, which is defined by v and $D_o$ (equation 5 [26]) that is in turn determined by Z (equation 4 [22]). Hence, laser scan at low v can process the metallic material at higher Z than laser scan at high v.

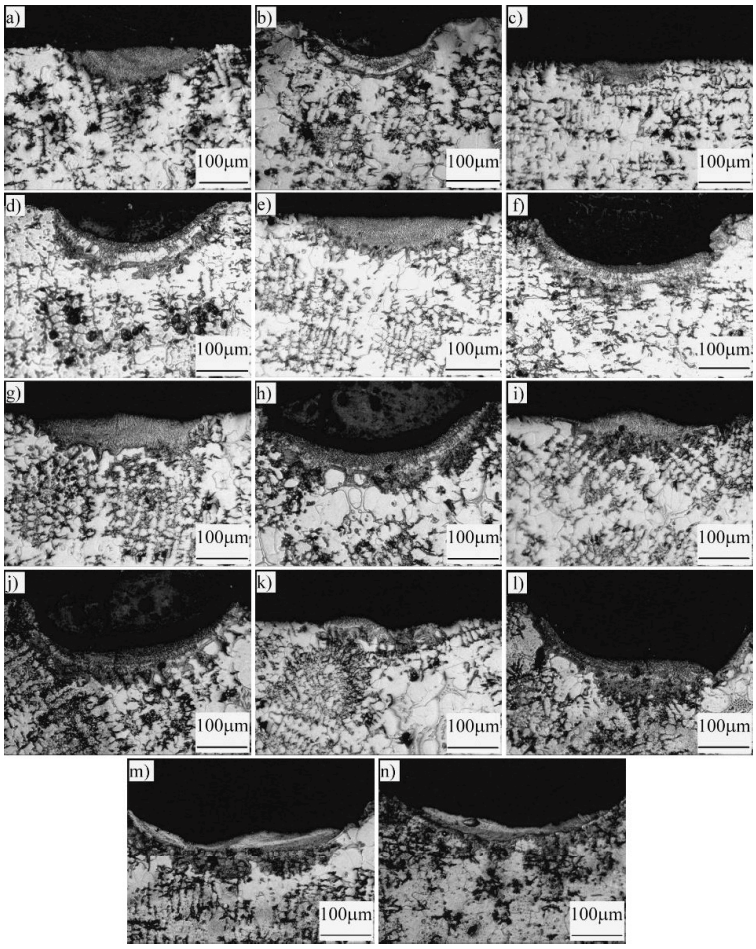


**Figure 2.** Optical pictures at 20X of sample cross-sections with a), c), e), g), i) and k) 5mm/s and b), d), f), h), j) and l-n) 1mm/s at a-b) 0mm, c-d) 0.8mm, e-f) 1.6mm, g-h) 2.4mm, i-j) 3.2mm, k-l) 4.0mm, m) 4.8mm and n) 5.6mm of distance to focal point.

Laser parameters influence on the width and depth of laser processed zones, can be observed in Figure 3. Influence behavior of these parameters were dissimilar for width than for depth. Laser scans at 1mm/s produced wider treated zones than that for laser scans at 5mm/s (Fig.3.a) because higher $E_l$ of 1mm/s laser scans. Width of the laser treated zone is exponentially proportional to $E_l$, as indicating the equation 6 [21, 28].

$$W^2 = D_o^2 * ln(\frac{E_l}{\varphi_{th}}) \quad (6)$$

Being, $\varphi_{th}$ energy fluence damage threshold. The behavior of the width with increment of Z is dissimilar for 1mm/s than that for 5mm/s. Regarding, 1mm/s, the increasing of Z increased the width because $D_o$ is proportional to Z (equation 4). In turn, width is linearly proportional to $D_o$, as being shown in equation 6 [21, 28]. Thus, the increasing of Z widens laser treated zones. This performance was also observed for Z form 0 to 2.4mm of the laser scans at 5mm/s .However, this behavior changed to opposite case for Z from 3.2-4.8. This is due is due to the reduction of the $E_l$ with increment of Z, as being viewed in equation 5 [26, 27]. At the same time, width is proportional to $E_l$ (equation 6 [21, 28]). Besides, the spatial distribution of the energy on laser beam is gaussian and therefore, edges of the laser spot have lower energy concentration than the centre [2, 21]. Thus, only laser spot centre have the enough energy density to modify the grey cast iron. Hence, the increment of Z reduces the width for these conditions.

Laser scans were wider at low v than that for high v because the $E_l$ is increased with the reduction of v (equation 5 [26, 27]). Equation 6 [21, 28] shows that width is exponentially proportional to $E_l$. The reduction of v therefore increases the width of laser scanned zone.

All laser scans had two different behaviors with the increasing of the Z that were defined by Z ranges, as can be seen in Figure 3.b. Z increasing deepened the treated zones for 0.0-3.2mm Z range in both v because the increment of $D_o$ increases the energy depth penetration, l. Depth of the laser processed zone, D, is proportional to l, as being shown in equation 7 [29].

$$D = l * ln(\frac{E_l}{\varphi_{th}}) \quad (7)$$

l is defined via thermal factor, $l_{therm}$, and optical parameter, $l_{op}$, as can be observed in equation 8 [30, 31].

$$l = l_{therm} + l_{op} \quad (8)$$

$l_{therm}$ is determined by thermodynamic properties of the material and laser parameters, as being detailed in equation 9 [30, 31]

$$l_{therm} = \sqrt{\xi * \beta * \tau} \quad (9)$$

Where, ξ is a geometric factor and τ is interaction time of the laser radiation on material. Meanwhile, $l_{op}$ is inversely proportional to absorption coefficient, α. In the case of the metallic materials processed with infrared laser, $l_{therm}$ is much larger than $l_{op}$ [30]. Thus, thermal factor is the dominant parameter in l. $l_{therm}$ is defined by τ (equation 9 [30, 31]), which is in turn determined through v and $D_o$, as can viewed in equation 10 [26].

$$\tau = \frac{D_o}{v} \quad (10)$$

As mentioned before, $D_o$ is dependent on Z (equation 4 [22]) and therefore, the increment of Z increases depth of laser treated zone.

Regarding laser scans at 5mm/s, treated zone depth with 3.2mm Z were smaller than for processed zone at 4.0mm Z. This due to lower $E_l$ and higher $\varphi_{th}$ for laser scans at 4.0mm.As commented early, the increment of Z reduces the $E_l$ that is determinant on the depth size. In the case of $\varphi_{th}$, larger Z generates higher values of this factor, as being indicated in equations 8 [30], 9 [30, 31], 10 [26] and 11 [29].

$$\varphi_{th} = E_{da} * l \quad (11)$$

Being, $E_d$ is the energy density damage threshold. As can be seen in equation 7 [29], the increment of $\varphi_{th}$ diminishes the depth of laser processed zones. Thus, the increment of Z reduces laser treated zone depth.

On regard laser scans at 1mm/s, laser processed zones at ≥3.2mm Z had similar depth because low v can offset the increment of $\varphi_{th}$ and the $E_l$ reduction. Although the increment of Z can diminish depth (equation 7 [29]) via $\varphi_{th}$ increasing (equation 11 [29]) and $E_l$ reducing, low v reduces the impact of these factors in the depth of the laser treated zones.

Laser processed zones had different microstructures that were dissimilar according to lase parameters, as can observed in microphotographs of Figure 4. Microstructures were classified as, Zone I, Zone II, Zone II, Zone IV, Zone V and Zone VI. Zone I was austenitic microstructure with undissolved flake graphite [10, 32]. The microstructure was pearlite with graphite flake [12] for Zone II. Microstructure of austenitic dendrite [3, 7] was viewed in Zone III whilst Zone IV had mixed microstructure that was consisted of austenitic matrix with martensitic structures and undissolved graphite [7]. Zone V also had a merged microstructures, austenite and martensitic [13, 33] while hypoeutectic dendritic microstructure [34] was seen in Zone VI. The last Zone, VII, was martensitic microstructure [3, 12].

Regarding laser scans at 5mm/s, laser treated samples had distinct number and type of Zones according to Z. Laser scans at focal point generated samples with only Zone I (Fig.4.a). Treated samples with two zones, Zone I and Zone II, were produced with laser scans at 0.8-3.2mm Z (Fig.4.c). Material processed with laser scans at 4.0mm Z had three zones; Zone III, Zone IV and Zone II (Fig.4.e).

On regard laser scans at 1mm/s, three distinct combinations of zones were observed. Treated samples at focal point and 0.8mm Z were consisted of Zone V, Zone IV and Zone II (Figure 4.b). Zone VI, Zone IV and Zone II formed the microstructures of the laser processed zones at 1.6mm and 2.4mm Z (Fig.4.d). The microstructure of the samples modified with 3.2mm and 4.0mm Z was similar to the previous microstructures but with graphite

flakes (Fig.4.f). Last microstructure was consisted of Zone VII, Zone I and Zone II, and this was found for samples treated with 4.8mm and 5.6mm Z (Fig.4.g).

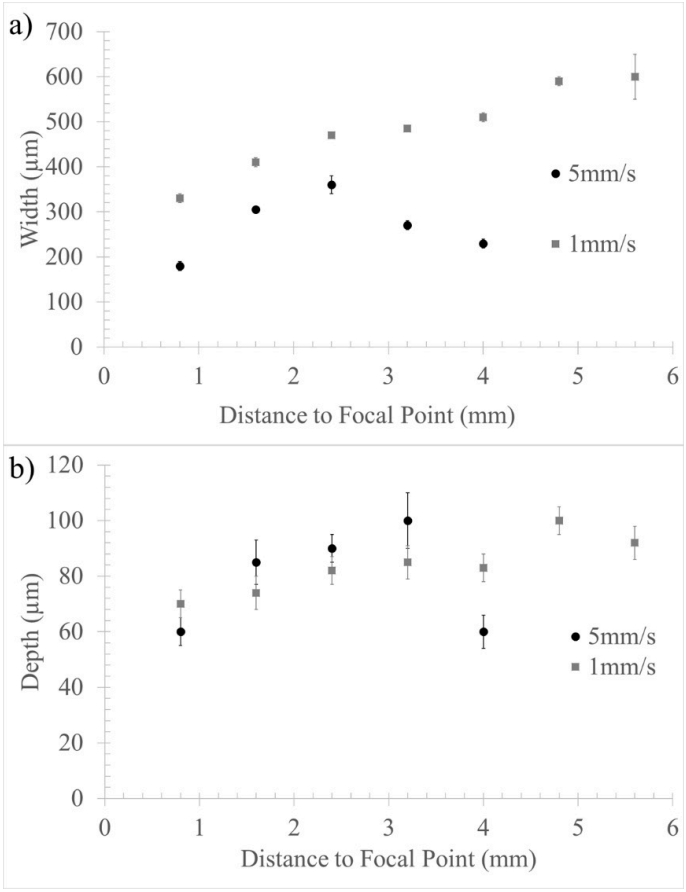


**Figure 3.** Graphs of a) width and b) depth of laser treated zone versus distance to focal point.

Various microstructures observed in the laser processed samples are due to the dissimilar temperatures that are reached by metallic materials according to depth and their distinct cooling times. Type of the microstructure is defined by both T and t [5, 13]. T is defined by laser parameters, depth of the laser treated zone, thermodynamic properties of the metallic material, as can be seen equation (12) [11, 17].

$$T = \frac{A*I}{\delta} * \sqrt{\xi * \beta * \tau} * ierfc\sqrt{\frac{Y^2}{\xi*\beta*\tau}} \tag{12}$$

Where, A is the absorptivity, I is the laser intensity and Y is the depth. Besides, I is determined by P and $D_o$, as can seen equation 13 [26].

$$I = \frac{P}{D_o^2} \tag{13}$$

T is proportional to I, A, β, τ and ξ, and is inversely proportional to Y, ε and $D_o$. On the other part, t is also determined by $D_o$, ξ, β and τ, as being viewed equation 14 [35].

$$t = \frac{D_o^2}{\sqrt{\xi*\beta*\tau}} \tag{14}$$

Thus, different microstructures can be found in a laser treated sample because temperatures of the material can be dissimilar to distinct depth [11, 17].

Microstructures can be designed via Z because this parameter also influences on t and T. Z is a determined factor on $D_o$ (equation 4 [22]) that in turn defines t and T. The increasing of $D_o$ reduces the T (equation 12 [11]) and increases t (equation 14 [35]).

Dissimilar microstructures according to v is due to this parameter also influences on t and T. These factors are determined by τ that is higher at slower laser scans. At longer τ is produced higher T (equation 12 [17]) and shorter t (equation 14 [35]).

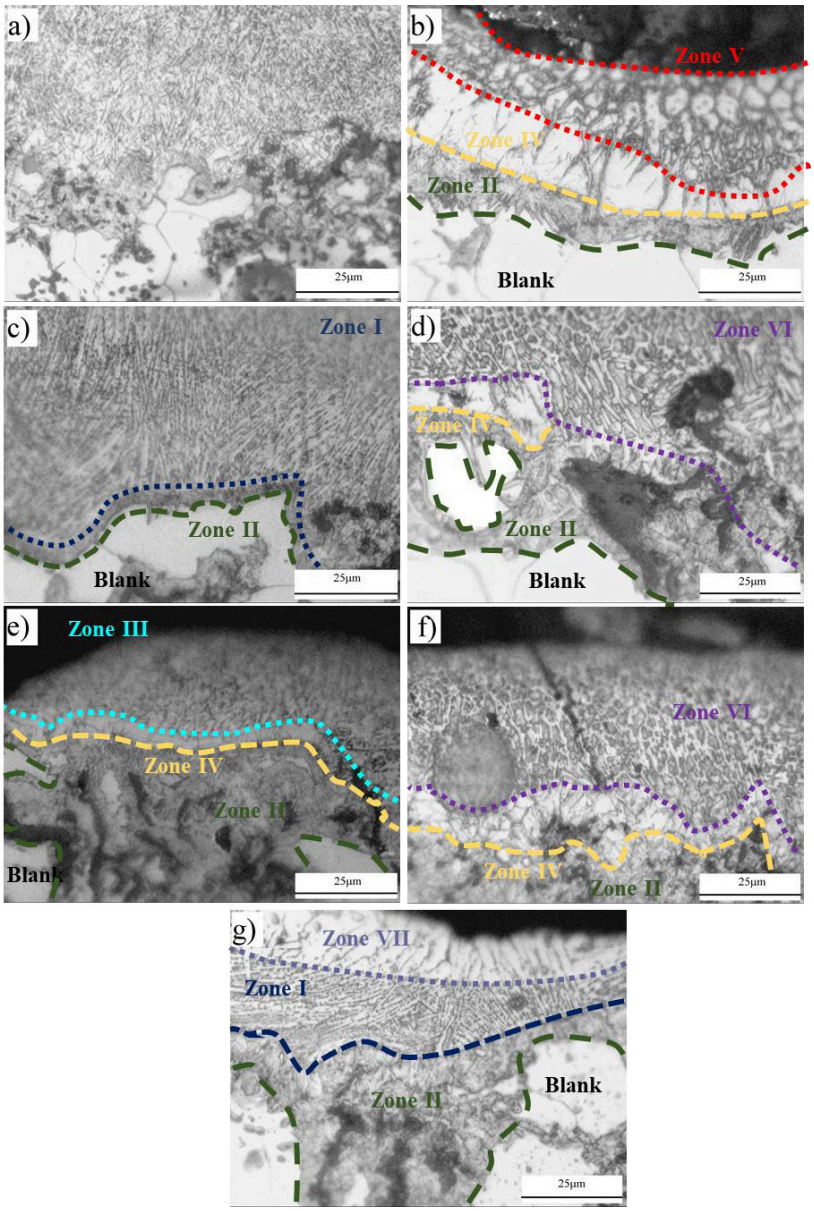


**Figure 4.** Optical pictures at 50X of the microstructures of samples treated with a), c), e) 5mm/s and b), d), f) and g) 1mm/s at a-b) focal point, c-d) 2.4mm, e-f) 4.0mm and g) 5.6mm Z.

## 4 Conclusions

Hardening via CW $C_2O$ laser can design the microstructure of the grey cast iron. The laser treated zone showed various types of the microstructures, e.g. martensitic (Zone VI and VII), austenitic (Zone V and Zone IV), dendrite

(Zone III) and pearlite (Zone II). The types of the microstructures were dissimilar according to the distance from focal point and scan speed. This can allow to design the microstructure of the grey cast iron and its physicochemical properties.

In addition, the size of the laser hardened or treated zones can be designed with laser parameters, distance from focal and scan speed. Slow scan speed, 1mm/s, generated larger laser treated zones than fast scan speed, 5mm/s. The increasing of the distance from focal point at slow scan speed enlarged laser hardened zone. However, all laser treated zones were ablated at 1mm/s. Laser scanning at 5mm/s were free of ablation but microstructural modification was only produced at ≤4.00mm of the distance of the focal point. Moreover, the increment of the distance from focal point increased the laser treated zone for ≤ 3.20mm, whilst the laser treated zone at 4.0mm was lower than laser hardened zone at 3.2mm. This study will permit to design the size of the laser hardened zone. In future work, the hardness, corrosion, wear and friction resistance of the laser treated zones will be evaluated to confirm the information obtained from literature.

**Reference**

[1] L. Collini, G. Nicoletto, R. Konečná, Microstructure and mechanical properties of pearlitic gray cast iron, Materials Science and Engineering: A 488 (2008) 529-539.
[2] A. Liu, B. Previtali, Laser surface treatment of grey cast iron by high power diode laser, Physics Procedia 5 (2010) 439-448.
[3] B. Wang, Y. Pan, Y. Liu, G.C. Barber, F. Qiu, M. Hu, Wear behavior of composite strengthened gray cast iron by austempering and laser hardening treatment, Journal of Materials Research and Technology 9 (2020) 2037-2043.
[4] O. Oloyede, T.D. Bigg, R.F. Cochrane, A.M. Mullis, Microstructure evolution and mechanical properties of drop-tube processed, rapidly solidified grey cast iron, Materials Science and Engineering: A 654 (2016) 143-150.
[5] M.J. Behnam, P. Davami, N. Varahram, Effect of cooling rate on microstructure and mechanical properties of gray cast iron, Materials Science and Engineering: A 528 (2010) 583-588.
[6] W.A. Monteiro, E. Silva, L. Silva, W. de Rossi, S. Buso, Microstructural and mechanical characterization of gray cast iron and AlSi alloy after laser beam hardening, Materials Science Forum, Trans Tech Publ, 2010, pp. 769-774.
[7] F. Fouquet, E. Szmatula, Laser surface melting of a pearlitic grey cast iron, Materials Science and Engineering 98 (1988) 305-308.
[8] B. Yilbas, I. Toor, C. Karatas, J. Malik, I. Ovali, Laser treatment of dual matrix structured cast iron surface: Corrosion resistance of surface, Optics and Lasers in Engineering 64 (2015) 17-22.
[9] M. Moradi, D. Ghorbani, M.K. Moghadam, M. Kazazi, F. Rouzbahani, S. Karazi, Nd: YAG laser hardening of AISI 410 stainless steel: Microstructural evaluation, mechanical properties, and corrosion behavior, Journal of Alloys and Compounds 795 (2019) 213-222.
[10] S. Lian, L. Chenglao, Effect of laser melting processing on the microstructure and wear resistance of gray cast iron, Wear 147 (1991) 195-206.
[11] P. Dinesh Babu, K. Balasubramanian, G. Buvanashekaran, Laser surface hardening: a review, International Journal of Surface Science and Engineering 5 (2011) 131-151.
[12] K. Sridhar, V. Katkar, P. Singh, J. Haake, Dry sliding friction wear behaviour of high power diode laser hardened steels and cast iron, Surface engineering 23 (2007) 129-141.
[13] E. Anusha, A. Kumar, S. Shariff, Diode laser surface treatment of bearing steel for improved sliding wear performance, Optik 206 (2020) 163357.
[14] R.J.B.D. Oliveira, R.H.M.D. Siqueira, M.S.F.D. Lima, Microstructure and wear behaviour of laser hardened SAE 4130 steels, International Journal of Surface Science and Engineering 12 (2018) 161-170.
[15] S. Martínez, A. Lamikiz, E. Ukar, A. Calleja, J. Arrizubieta, L.L. de Lacalle, Analysis of the regimes in the scanner-based laser hardening process, Optics and Lasers in engineering 90 (2017) 72-80.
[16] B. Wu, T. Ozel, Micro-laser processing, Micro-Manufacturing: Design and Manufacturing of Micro-Products, John Wiley and Sons2011, pp. 159-195.
[17] F. Vollertsen, K. Partes, J. Meijer, State of the art of Laser Hardening and Cladding, Proceedings of the 3th International WLT-Conference on Lasers in Manufacturing, 2005.
[18] D. Patel, P. Nanavati, C. Chug, Effect of Ca and Ba Containing Ferrosilicon Inoculants on Microstructure and Tensile Properties of IS-210, and IS-1862 Cast Irons.
[19] A.S.f.T.a. Materials, Standard Specification for Gray Iron Castings, ASTM A48 / A48M - 00, ASTM International, West Conshohocken, 2000, pp. 5.

[20] K. Hellström, P. Svidró, L.V. Diaconu, A. Diószegi, Density Variations during Solidification of Grey Cast Iron, Materials Science Forum, Trans Tech Publ, 2018, pp. 155-162.
[21] E. Williams, E. Brousseau, Nanosecond laser processing of Zr41. 2Ti13. 8Cu12. 5Ni10Be22. 5 with single pulses, Journal of Materials Processing Technology 232 (2016) 34-42.
[22] A.G. Demir, B. Previtali, N. Lecis, Development of laser dimpling strategies on TiN coatings for tribological applications with a highly energetic Q-switched fibre laser, Optics & Laser Technology 54 (2013) 53-61.
[23] D. Sola, A. Conde, I. García, E. Gracia-Escosa, J.J. De Damborenea, J.I. Peña, Microstructural and wear behavior characterization of porous layers produced by pulsed laser irradiation in glass-ceramics substrates, Materials 6 (2013) 3963-3977.
[24] M. Moradi, E. Golchin, Investigation on the effects of process parameters on laser percussion drilling using finite element methodology; statistical modelling and optimization, Latin American Journal of Solids and Structures 14 (2017) 464-484.
[25] A. International, Standard Practice for Microetching Metals and Alloys Produced by ASTM, ASTM International2011.
[26] W. Suder, S. Williams, Investigation of the effects of basic laser material interaction parameters in laser welding, Journal of laser applications 24 (2012) 032009.
[27] T. Heiderscheit, N. Shen, Q. Wang, A. Samanta, B. Wu, H. Ding, Keyhole cutting of carbon fiber reinforced polymer using a long-duration nanosecond pulse laser, Optics and Lasers in Engineering 120 (2019) 101-109.
[28] A. Žemaitis, P. Gečys, M. Barkauskas, G. Račiukaitis, M. Gedvilas, Highly-efficient laser ablation of copper by bursts of ultrashort tuneable (fs-ps) pulses, Scientific reports 9 (2019) 1-8.
[29] B. Neuenschwander, B. Jaeggi, M. Schmid, A. Dommann, A. Neels, T. Bandi, G. Hennig, Factors controlling the incubation in the application of ps laser pulses on copper and iron surfaces, Laser Applications in Microelectronic and Optoelectronic Manufacturing (LAMOM) XVIII, International Society for Optics and Photonics, 2013, pp. 86070D.
[30] X. Liu, D. Du, G. Mourou, Laser ablation and micromachining with ultrashort laser pulses, IEEE journal of quantum electronics 33 (1997) 1706-1716.
[31] S. Ullah, A. Dogar, H. Qayyum, Z. Rehman, A. Qayyum, The influence of surface contamination on the ion emission from nanosecond-pulsed laser ablation of Al and Cu, Journal of Physics D: Applied Physics 51 (2018) 165602.
[32] B. Wang, G.C. Barber, R. Wang, Y. Pan, Comparison of Wear Performance of Austempered and Quench-Tempered Gray Cast Irons Enhanced by Laser Hardening Treatment, Applied Sciences 10 (2020) 3049.
[33] X. Tong, H. Zhou, M. Liu, M.-j. Dai, Effects of striated laser tracks on thermal fatigue resistance of cast iron samples with biomimetic non-smooth surface, Materials & Design 32 (2011) 796-802.
[34] L. Elmquist, S. Salera, A. Diószegi, Inoculation and its effect on primary solidification structure of hypoeutectic grey cast iron, International Journal of Cast Metals Research 23 (2010) 124-129.
[35] G. Eberle, M. Schmidt, F. Pude, K. Wegener, Laser surface and subsurface modification of sapphire using femtosecond pulses, Applied Surface Science 378 (2016) 504-512.